Available online at www.sciencedirect.com
SCIENCE DIRECT®
International Journal of Heat and Mass Transfer 47 (2004) 717–728
International Journal of HEAT and MASS TRANSFER
www.elsevier.com/locate/ijhmt

Heat transfer in scraped eutectic crystallizers

R.J.C. Vaessen, M.M. Seckler, G.J. Witkamp *

Laboratory for Process Equipment, Delft University of Technology, Leeghwaterstraat 44, 2628 Delft CA, The Netherlands

Received 13 January 2003; received in revised form 18 July 2003

Abstract

Heat transfer phenomena in two types of eutectic crystallizers have been analyzed. This equipment is equipped with rotating scraper blades and the effect of the blade action on heat transfer phenomena in both crystallizing and non-crystallizing conditions is studied. It was found that the coolant flow in the equipment can be described by fitted Dittus–Boelter relations. In both crystallizers the transport of heat from process liquid to cooled wall surfaces at various rotational speeds of the scrapers can generally be accurately described with penetration theory. Exceptions are approximated with fitted *Re–Pr*-relations. Both increasing and decreasing heat transfer rates have been found in crystallizing conditions at increasing scraping rates. Differences are attributed to geometrical crystallizer characteristics and solid content.

1. Introduction

Heat transfer plays an important role in the performance of eutectic crystallizers as it determines the production capacity. Previous work has shown that the temperature difference between coolant and process fluid should not exceed a critical value. Therefore supersaturation is the limiting factor in eutectic crystallization processes. The scraper action needed for the removal of ice from the cooled surface also improves heat transfer. Others have investigated the heat transfer properties of scraped surface heat exchangers (SSHE) [1–6]. Since this type of equipment is generally characterized by a tubular geometry with a small diameter–length ratio in which the process liquid has a high axial velocity, flow phenomena differ from the processes within the eutectic crystallizers. However the principal of cooling a liquid through scraped metal surfaces is similar in both scraped surface heat exchangers and eutectic crystallizers. The approach in modeling heat transfer for SSHE's is therefore also applied for eutectic crystallizers. This paper discusses the heat transfer resistances in the crystallizer equipment. The geometry of the cooled disc column crystallizer (CDCC) and scraped cooled wall crystallizer (SCWC) is described, defining characteristic lengths in heat transfer relations and dimensionless numbers. Based on expected flow regimes in coolant and process fluid the theoretical backgrounds of heat transfer phenomena for both sides are discussed. The heat transfer behavior for both types of crystallizers are determined experimentally and modeled. A thorough characterization has taken place using water and a ternary KNO_3–HNO_3 solution as a process liquid in non-crystallizing conditions. The obtained relations are then compared to crystallizing experiments, in which the presence of crystals significantly affect physical properties of the process medium.

2. Heat transfer resistances

It is reasonable to simplify the total heat transfer from the coolant to the process medium within the crystallizer as a one-dimensional stationary process. In this case the total amount of transferred energy per square meter of cooled surface per second (Q_{tot}) is directly related to the temperature difference between coolant and process liquid:

* Corresponding author. Tel.: +31-15-278-3602; fax: +31-15-278-6975.
E-mail address: g.j.witkamp@wbmt.tudelft.nl (G.J. Witkamp).

0017-9310/$ - see front matter © 2003 Elsevier Ltd. All rights reserved.
doi:10.1016/j.ijheatmasstransfer.2003.07.028

Nomenclature

a	exponent (dimensionless)
b	exponent (dimensionless)
C	constant (dimensionless)
C_p	heat capacity ($J\,kg^{-1}\,K^{-1}$)
D	diameter (m)
h	height (m)
K	constant ($m^2\,K\,W^{-1}$)
N	rotational speed (s^{-1})
n	number of scrapers (dimensionless)
Q	heat flux ($W\,m^{-2}$)
R^2	coefficient of determination (dimensionless)
T	temperature (°C)
t	thickness (m)
t	time (s)
w	width (m)
y	length (m)

Dimensionless numbers

Nu	Nusselt
Pr	Prandtl
Re	Reynolds

Greek symbols

α	heat transfer coefficient ($W\,m^{-2}\,K^{-1}$)
Δ	difference (dimensionless)
η	dynamic viscosity (Pa s)
λ	thermal conductivity ($W\,m^{-1}\,K^{-1}$)
ρ	density ($kg\,m^{-3}$)
ϕ	volumetric flow ($m^3\,s^{-1}$)

Subscripts

bulk	bulk
coolant	coolant
cool,in	entering coolant
cool,out	outgoing coolant
cryst	crystallizer
hydr	hydraulic
in	inner cylinder
log	logarithmic
min	minimal
out	outer cylinder
pen	penetration
plate	plate
process	process
rect. duct	rectangular duct
s	scraper passage
scraper	scraper
therm	thermal
tot	total
turb	turbulent
wall	wall

$$Q_{\text{tot}} = \alpha_{\text{tot}} \cdot \Delta T_{\text{coolant–process}} \tag{1}$$

Since the temperature of the coolant may increase up to 2 K during its transport through the equipment, the driving of the temperature difference is best expressed by the logarithmic mean temperature difference:

$$\Delta T_{\text{coolant–process}} = \frac{T_{\text{cool,out}} - T_{\text{cool,in}}}{\ln\left(\frac{T_{\text{cool,out}} - T_{\text{cryst}}}{T_{\text{cool,in}} - T_{\text{cryst}}}\right)} \tag{2}$$

The total heat transfer resistance depends on the resistances within coolant, scraped surface and process liquid. This is depicted in Fig. 1 and expressed in Eq. (3):

$$\frac{1}{\alpha_{\text{tot}}} = \frac{1}{\alpha_{\text{coolant}}} + \frac{1}{\alpha_{\text{plate}}} + \frac{1}{\alpha_{\text{process}}} \tag{3}$$

The separate resistances are either a material property or ruled by flow phenomena. Since in experiments only the

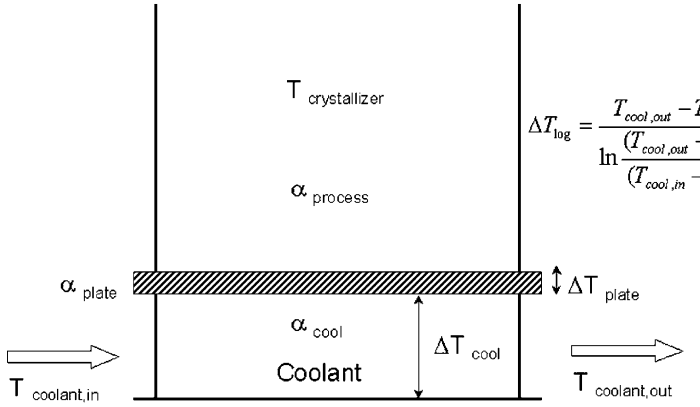

Fig. 1. Schematic overview of heat transfer resistances in coolant, scraped surface and process liquid.

total heat transfer coefficient can be measured, single resistances are to be determined from experiments varying one single resistance. The results of these measurements are discussed in the following paragraphs of this paper.

3. Crystallizer geometry and definition of dimensionless numbers

The following section is dedicated to the geometric description of the CDCC and the SCWC and the definition of several dimensionless numbers used in heat transfer relations.

3.1. Cooled disc column crystallizer

Heat in the CDCC is transferred by horizontal double-sided discs made of stainless steel. To ensure an even distribution of coolant flow through the discs a labyrinth-shaped trajectory is constructed, as depicted in Fig. 2. This trajectory can be regarded as a curved duct with a height of 20 mm and a width of 60 mm. Coolant flow rates ranged from 1.4×10^{-4} to 2.8×10^{-4} $m^3\,s^{-1}$. The Reynolds number of the coolant (Freezium™), calculated with a hydraulic diameter of 30 mm of the duct, lies between 900 and 1900. This means the flow regime is in transition between laminar and turbulent flow ($Re_{turbulent} > 10^4$). Heat transfer relations described in literature for laminar/turbulent flow in ducts or tubes might be applicable.

The metal plates in the cooled disc have a thickness of 4 mm. Since the thermal conductivity of stainless steel is related to its temperature, a linear equation of the form $(aT + b)$ is derived from measurements on SS-316 [7]. The constants in this equation are stated in Table 1.

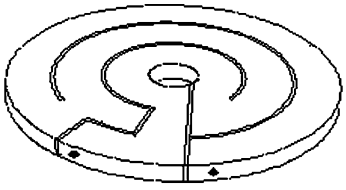

Fig. 2. Internal geometry of a cooled element within the CDCC.

Table 1
Constants a and b in the linear relation for calculation of thermal conductivity of SS-316 as a function of temperature in °C

Parameter	Value	Unit
a	0.0265	$W\,m^{-1}\,K^{-2}$
b	14.593	$W\,m^{-1}\,K^{-1}$

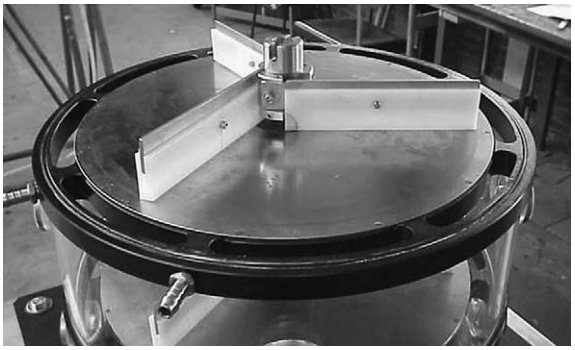

Fig. 3. Open view of a cooled element with three mounted scrapers.

It results in a thermal conductivity of the cooled plates ranging from 14.2 $W\,m^{-1}\,K^{-1}$ at −15 °C to 15.4 $W\,m^{-1}\,K^{-1}$ at 30 °C.

The geometry of the CDCC on the process side is shown in Fig. 3 of the disassembled crystallizer. Flow phenomena above the cooled disc on the process side are influenced by the action of the scrapers. Due to their height of approximately 50 mm scraping simultaneously results in mixing. The flow regime as a result of mixing or stirring is generally expressed by the rotational Reynolds number:

$$Re_{rot} = \frac{\rho_{process} \cdot N \cdot D^2_{scraper}}{\eta_{process}} \tag{4}$$

where N is the scraping rate and D is the diameter of the scraper blades (400 mm).

Since the direction of heat transfer is perpendicular to the cooled plate, the characteristic length used for the calculation of the Nusselt number is defined by the height of a column compartment (140 mm). Experiments have been performed with a CDCC configuration consisting of four compartments and three cooled elements, having a volume of approximately 110 l.

3.2. Scraped cooled wall crystallizer

The SCWC consists of a cylindrical vessel with a cooled wall. In order to increase the cooling capacity a second cooled cylinder is placed within the crystallizer. An even distribution of the coolant flow throughout each jacket is ensured by a spiral-shaped path. A crosscut of the jacketed wall's internal geometry is depicted in Fig. 4. The dimensions, calculated hydraulic diameters and the Reynolds number range of the inner and outer jacket are indicated in Table 2. Coolant flow rates were set in the range of 2.0×10^{-4} to 2.8×10^{-4} $m^3\,s^{-1}$. Coolant Reynolds numbers are obtained of 3000–4000. The coolant flow regime is situated in

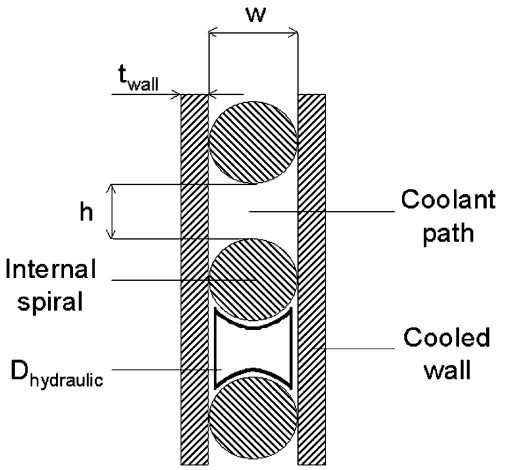

Fig. 4. Internal geometry of the cooled jacket of the SCWC showing cooled wall and internal spiral for proper coolant distribution.

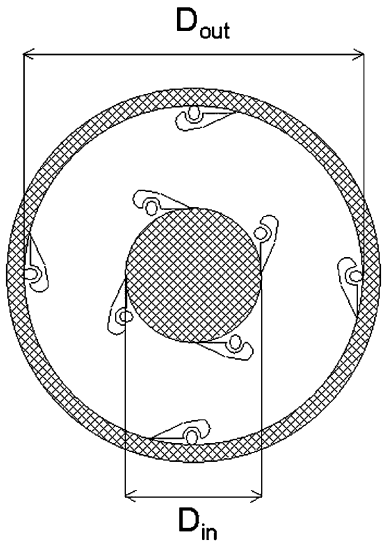

Fig. 5. Top view of the SCWC with inner and outer cooled wall each equipped with four scrapers.

Table 2
Dimensions and Reynolds number of coolant trajectory in SCWC wall and inner cylinder (symbols are defined in Fig. 4)

Parameter	Outer jacket	Inner jacket	Unit
w	10	10	mm
h	30	20	mm
$D_{hydraulic}$	12.2	10	mm
t_{wall}	10.0	9.45	mm
Re	2000–3500	2400–4000	–

transition area between laminar and turbulent flow. Heat transfer relations for laminar/turbulent flow in curved tubes are considered for validation. The crystallizer volume consists of an annular space between the crystallizer wall (D_{out}: 500 mm) and the inner cooled cylinder (D_{in}: 200 mm). Each cooled surface is in contact with four scrapers mounted on a rotating cage-like structure. A top view of the internal geometry of the SCWC is provided in Fig. 5.

The turbulence within the crystallizer is expressed by a rotational Reynolds number adjusted for annular equipment, considering the scraper speed at the outer jacket of the crystallizer and the size of the largest turbulent swirl fitting in the annulus:

$$Re_{rot} = \frac{\rho_{process} \cdot N \cdot (D_{out} - D_{in})^2}{\eta_{process}} \quad (5)$$

The characteristic length of heat transfer in calculations of Nusselt numbers is determined by the annular space between inner and outer cylinder and has a value of 150 mm.

4. Theory

This section gives an overview of models and empirical relations used for heat transfer calculations. Appropriate models are empirical relations for flows in tubes and ducts for the coolant and penetration theory and *Re–Pr*-relations for the process medium side. Most of these models use dimensionless expressions in which the Nusselt number represents the heat transfer by

$$Nu = \frac{\alpha \cdot D}{\lambda} \quad (6)$$

4.1. Heat transfer in tubes and ducts

Heat transfer relations in the CDCC and the SCWC are evaluated in which the tube diameter is replaced by the hydraulic diameter. If the coolant flow is in the laminar regime analytical solutions can be derived for heat transfer, represented by the following Nusselt number [8] for fully developed tube flow:

$$Nu_{tube} = 3.66 \quad (7)$$

And for a rectangular duct with a height/width-ratio of 1/3 with uniform heat flux through top and bottom and insulated side walls:

$$Nu_{rect.\ duct} = 6 \quad (8)$$

For turbulent flow in tubes a classical correlation is derived by Dittus and Boelter [9].

There are slight differences between flows being heated or cooled, respectively:

$$Nu_{\text{heated}} = 0.026 \cdot Re^{0.8} \cdot Pr^{0.4} \tag{9}$$

$$Nu_{\text{cooled}} = 0.024 \cdot Re^{0.8} \cdot Pr^{0.3} \tag{10}$$

Relations (9) and (10) are developed for Prandtl numbers between 0.7 and 120 and Reynolds numbers of 2.5×10^3 up to 1.24×10^5. The objective of the derivation of two different relations for cooling and heating is to account for the variation of physical properties.

4.2. Heat transfer from scraped surfaces

A basic physical approach of heat transfer from a scraped plate into a liquid is provided by the penetration theory [12]. The theory is based on conductive heat transfer, meaning flow phenomena and viscosity of the process medium have no influence. The heat transfer process is divided into the following steps:

- Heat penetrates by conduction into a stagnant boundary layer above the heat transfer surface.
- As a scraper blade passes, the laminar boundary layer is removed.
- The removed boundary layer mixes completely and instantaneously with the bulk.
- The newly replaced layer has a temperature equal to the bulk temperature.

Heat penetration is expressed by the Fourier equation for conductive heat in y-direction:

$$\frac{\partial T}{\partial t} = \frac{\lambda}{\rho \cdot C_{\text{p}}} \cdot \frac{\partial^2 T}{\partial y^2} \tag{11}$$

with boundary conditions:

$$y = 0, \quad T = T_{\text{wall}}; \quad y \to \infty, \quad T = T_{\text{bulk}} \tag{12}$$

and initial condition

$$t = 0, \quad T = T_{\text{bulk}} \tag{13}$$

Solving the differential equation and substituting into the relation for transferred heat delivers:

$$Q = -\lambda \cdot \frac{\partial T}{\partial y} = (T_{\text{bulk}} - T_{\text{wall}}) \cdot \sqrt{\frac{\lambda \cdot \rho \cdot C_{\text{p}}}{\pi \cdot t}} \tag{14}$$

Then the heat transfer coefficient is given by

$$\alpha(t) = \sqrt{\frac{\lambda \cdot \rho \cdot C_{\text{p}}}{\pi \cdot t}} \tag{15}$$

The time averaged heat transfer coefficient in between scraper passages (t_{s}) is

$$\bar{\alpha} = \frac{1}{t_{\text{s}}} \cdot \int_0^{t_{\text{s}}} \alpha(t)\,\mathrm{d}t = n \cdot N \cdot \int_0^{t_{\text{s}}} \sqrt{\frac{\lambda \cdot \rho \cdot C_{\text{p}}}{\pi \cdot t}}\,\mathrm{d}t = 2 \cdot \sqrt{\frac{\lambda \cdot \rho \cdot C_{\text{p}} \cdot n \cdot N}{\pi}} \tag{16}$$

In order to describe the total heat transfer process with this relation the time in between two scraper passages should be smaller or at least equal to the time needed for full penetration of heat into the boundary layer. The penetration depth is characterized by

$$\delta_{\text{pen}} = \sqrt{\frac{\pi \cdot \lambda \cdot t}{\rho \cdot C_{\text{p}}}} \tag{17}$$

Thus the time required for the development of a layer with penetration depth δ_{pen} is

$$t_\delta = \frac{\delta_{\text{pen}}^2 \cdot \rho \cdot C_{\text{p}}}{\pi \cdot \lambda} \tag{18}$$

A fully developed thermal boundary layer in turbulent flow has a thickness of

$$\delta_{\text{therm,turb}} = \frac{\lambda}{\alpha_{\text{turb}}} \tag{19}$$

In which α_{turb} is the turbulent heat transfer coefficient. Substituting this into Eq. (18) for calculation of the thermal boundary development time and expressing the time in terms of the scraping rate and the number of scrapers, the minimum rotational speed is known:

$$N_{\min} = \frac{\pi \cdot \alpha_{\text{turb}}^2}{n \cdot \lambda \cdot \rho \cdot C_{\text{p}}} \tag{20}$$

If the applied rotational speed is lower than this minimum value, the heat transfer is ruled by a combination of heat penetration and heat transfer in a turbulent flowing medium. In the first part of the process, until t_δ, heat transfer is governed by penetration. In the remaining period until the next scraper blade passes at t_{s}, turbulent flow ϕ determines the heat transfer. The time averaged heat transfer coefficient of Eq. (16) is then adjusted to

$$\bar{\alpha}(N,\phi) = \frac{1}{t_{\text{s}}}\left[\int_0^{t_\delta} \alpha_{\text{pen}}(t)\,\mathrm{d}t + \int_{t_\delta}^{t_{\text{s}}} \alpha_{\text{turb}}(\phi)\,\mathrm{d}t\right] \tag{21}$$

Substitution of Eqs. (15) and (18) and expressing t_{s} by the scraping rate, delivers the following equation:

$$\bar{\alpha}(N,\phi) = \frac{n \cdot \lambda \cdot \rho \cdot C_{\text{p}}}{\pi \cdot \alpha_{\text{turb}}(\phi)} N + \alpha_{\text{turb}}(\phi) \tag{22}$$

Penetration theory adjusted with correction factors has been successfully used by several researchers in the past to describe heat transfer phenomena in scraped surface heat exchangers. More details on this can be found in the dissertations of Trommelen [11] and de Goede [10].

Fluid dynamics and heat conductivity have a major influence on heat transfer processes are fluid dynamics. These phenomena can be characterized by parameters like density, viscosity, velocity, temperature differences and heat capacity. It is common practice to express these

quantities in terms of dimensionless Reynolds, Prandtl and Nusselt numbers in the following form:

$$Nu = C \cdot Re^{a} \cdot Pr^{b} \tag{23}$$

where the exponent of the Reynolds number usually has a value between 0.5 and 1 and the exponent of the Nusselt number is often set to 0.3. For processes in transient regimes or situations in which a combination of physical heat transfer principles can be distinguished, this type of relation has been proven to be useful.

5. Heat transfer in CDCC

5.1. CDCC coolant heat transfer characterization

Heat transfer characteristics of the coolant in the CDCC have been determined in experiments with constant process side conditions, i.e. constant scraping rate while coolant flow rates were varied in the range of 0.39–1.00 $m^3\,h^{-1}$ per cooled element. The resulting total heat transfer rates in experiments performed with water as the process fluid are depicted in Fig. 6. Since process conditions are equal the increase in heat flux can be attributed solely to the higher coolant flow rates within the cooled disc. The fact that heat transfer depends on coolant flow rate proves that the heat transfer cannot be represented by a laminar model. By replacing the terms in Eq. (3), representing the heat transfer resistance in the metal plate and process medium by a single constant K, a flow rate dependent relation for α_{cool} can be derived. The Dittus and Boelter relation stated in Eq. (9) was taken as a starting point for obtaining a model. The power of the Prandtl number is set at 0.3. The pre-exponential term was fitted to our experimental data using the least squares method on

$$\frac{1}{\alpha_{tot}} = \frac{D_{hydr}}{C \cdot Re^{0.8} \cdot Pr^{0.3} \cdot \lambda} + K \tag{24}$$

The following constant C was thus derived for the Dittus and Boelter relation:

$$Nu = 0.086 \cdot Re^{0.8} \cdot Pr^{0.3} \tag{25}$$

5.2. CDCC process heat transfer characterization

Since the heat transfer resistance of the metal plate and the coolant are known, the process side heat transfer coefficient can be calculated from the measured total heat transfer coefficient. Experiments have been performed in which both water and a ternary HNO_3–KNO_3 solution were cooled from 18 to 8 °C at different scraping rates. Water was used as a model system since its physical properties as a function of temperature are known, enabling calculation of accurate temperature dependent Reynolds and Prandtl numbers. The results of the heat transfer measurements are depicted in Fig. 7 for both systems. Reynolds numbers are calculated with Eq. (4). The data points seem to be grouped which is due to the different scraping rates, ranging from 0.13 to 0.63 rev s^{-1}, at which the experiments were performed. Reynolds numbers at a certain scraping rate depend on the water temperature and therefore span over a Reynolds number range, as is shown in Fig. 7. Nusselt numbers for the HNO_3–KNO_3 system are lower than for water at equal Reynolds values, which can be explained by the fact that heat capacity and thermal conductivity of this solution are lower. Theoretically being the most appropriate physical model for heat transfer phenomena in the scraped eutectic crystallizers, penetration theory has been evaluated first on its applicability, before an em-

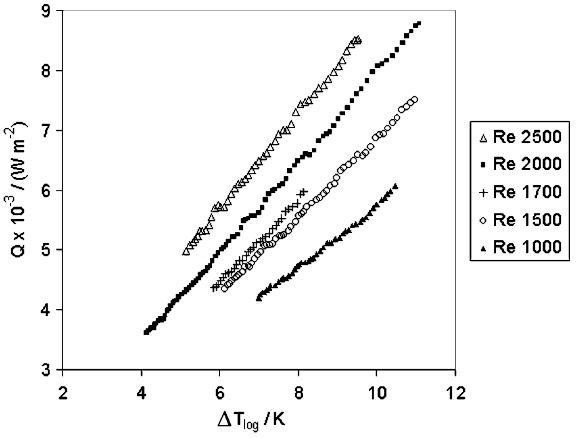

Fig. 6. Total heat transfer at different coolant flow rates expressed by *Re*-number.

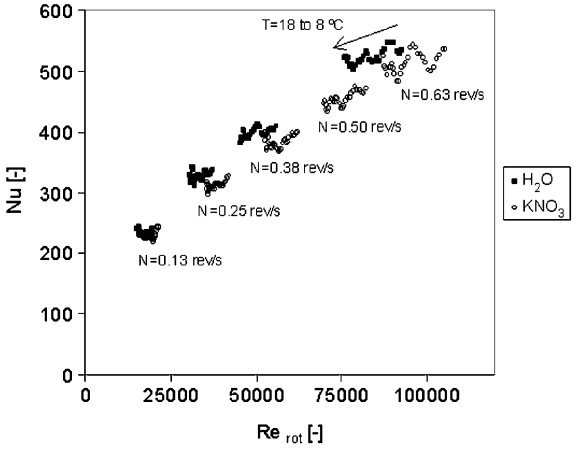

Fig. 7. Process side Nusselt numbers for water and KNO_3–HNO_3 solution cooled from 18 to 10 °C at different scraping rates.

pirical model Reynolds–Prandtl relation has been derived.

5.3. CDCC heat transfer in non-crystallizing conditions

In order to examine if heat transfer is merely determined by penetration theory, Eq. (22) must be solved knowing the time averaged heat transfer coefficient from experiments and α_{turb} being the unknown parameter. Since no real solutions existed for α_{turb}, it is concluded that heat penetration is the dominating phenomenon. In other words experiments were continuously performed at scraping rates higher than the required minimum rotational speed. The applicability of the penetration theory has been tested by comparing experimental heat transfer rates of water and KNO_3–HNO_3 solution with the following relation:

$$\alpha_{process} = C_{pen} \cdot \sqrt{\frac{\lambda \cdot \rho \cdot C_p \cdot n \cdot N}{\pi}} \tag{26}$$

The constant C_{pen} has been fitted with the least squares method and delivered a value of 1.79. The coefficient of determination of the fitted constant is 0.989. The fitted constant deviates approximately 10% from the theoretically calculated factor of 2 (see Eq. (16)). This can be attributed to the fact that complete and immediate mixing as assumed in the model is not attained in practice.

Application of the penetration theory implies that strongly temperature related properties like viscosity play no role in the heat transfer process. In order to physically comply with this assumption isothermal curves have been prepared from measurements at equal process side temperatures. Nusselt numbers comparing model calculations from Eq. (26) and experimental values for temperatures of 17 and 10 °C are depicted in Fig. 8 for water and Fig. 9 for the ternary electrolyte solution. Inspection of Eq. (26) shows that the slight differences in heat transfer rate are a consequence of the temperature dependence of thermal conductivity, density and heat capacity. The graphs show that heat transfer predictions according to penetration theory agree well with experimental results.

By linearization of Eq. (23) regression an optimal fit is determined for parameters a, b and C for the heat transfer experiments depicted in Fig. 7. This delivered the values stated in Table 3. Since Nusselt shows a squared root dependency with Reynolds and in literature a Prandtl exponent of 1/3 is commonly mentioned, a fit has also been produced only deriving constant C. The result is also mentioned in Table 3 under 'C fit'. The difference in accuracy between these two fits is expressed by the coefficient of determination R^2.

The fact that the exponent of the Reynolds number is close to 1/2 in both cases stresses the applicability of penetration theory. This empirical function is however more accurate since it includes the effect of viscosity and its temperature dependence, represented in both dimensionless numbers. In Fig. 10 experimental Nusselt numbers of water which is cooled from 18 to 10 °C at scraping rates of 0.38 and 0.62 rev s^{-1} are shown and are

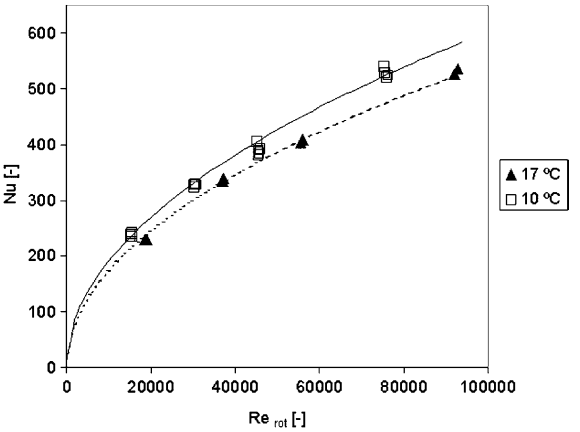

Fig. 8. Experimental process side Nusselt numbers for water compared to calculated values using fitted penetration theory at 17 and 10 °C represented by lines ($C_{pen} = 1.79$).

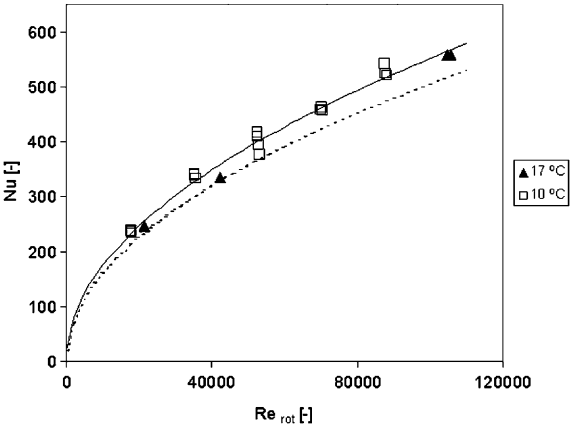

Fig. 9. Experimental process side Nusselt numbers for KNO_3–HNO_3 solution compared to calculated values using fitted penetration theory at 17 and 10 °C represented by lines ($C_{pen} = 1.79$).

Table 3
Fitted parameters in the Reynolds–Prandtl heat transfer relation for the CDCC

Parameter	Total fit	C fit
a	0.504	0.500
b	0.426	0.333
C	0.684	0.867
R^2	0.992	0.989

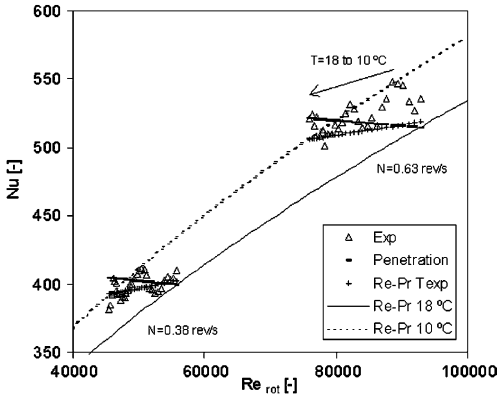

Fig. 10. Comparison of penetration theory and *Re–Pr*-relation for water cooled from 18 to 10 °C at 0.38 and 0.62 rev s^{-1}.

compared to penetration theory and the fitted *Re–Pr*-relation. Each presented value for both penetration theory and the *Re–Pr*-relation corresponds to an experimental data point, indicated with triangles. Isothermal curves for 10 and 18 °C over the whole Reynolds range are also depicted. Although both the penetration and *Re–Pr*-model provide reasonable heat transfer predictions it is clear that the trend of the *Re–Pr*-relation is more in accordance with experimental data.

5.4. CDCC heat transfer in crystallizing conditions

Experiments with an aqueous ternary solution containing KNO_3 and HNO_3 in eutectic conditions have been performed in the CDCC. In this situation ice and potassium nitrate are formed simultaneously. Thus the main part of transferred heat is consumed by the formation of these solid phases. The CDCC contains approximately 8 wt.% of solids. Ice crystals typically have a flat circular disc shape, with sizes ranging from 100 to 200 μm. The potassium nitrate particles are agglomerates of well faceted primary crystals and have average sizes of 100–200 μm.

Heat fluxes ranged from 0.6 to 6.6 kW m^{-2} at logarithmic temperature differences between coolant and process fluid from 2 to 10 °C. The top plate, from the three in total present in the CDCC, shows an overall heat transfer coefficient of approximately 540 W m^{-2} K^{-1}, while the middle element transfers 720 W m^{-2} K^{-1}. These values are obtained by calculating the slope of the linear heat transfer curve over a range of logarithmic temperature differences between 2 and 10 K. The lower heat transfer in the top section of the crystallizer might be a result of the presence of large amounts of ice crystals hampering efficient bulk mixing.

In order to prevent formation of ice scale layers the scraping rate was increased with increasing logarithmic temperature difference. This means that the increase in heat flux is not only the result of a larger temperature difference but also of an increased scraper speed. It is therefore physically more correct to express the heat flux as a function of the product of logarithmic temperature difference and the square root of the scraping rate in Fig. 11, assuming heat transfer corresponding to penetration theory in crystallizing conditions. In contrast to the heat flux curves versus the temperature difference, the intercepts of the linear relations in Fig. 11 are located at 0. Further analysis of heat transfer data leads to the process side heat transfer coefficient, shown in Fig. 12. The fact that the process side heat transfer coefficient is proportional to the square root of the scraping rate confirm the applicability of penetration theory in crystallizing conditions in the CDCC at a constant crystal-

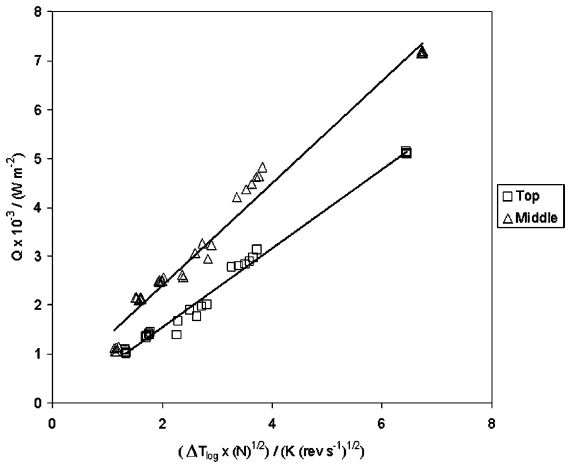

Fig. 11. Heat fluxes of top and middle cooled plate versus product of logarithmic temperature difference and square root of the scraping rate in the CDCC under crystallizing conditions.

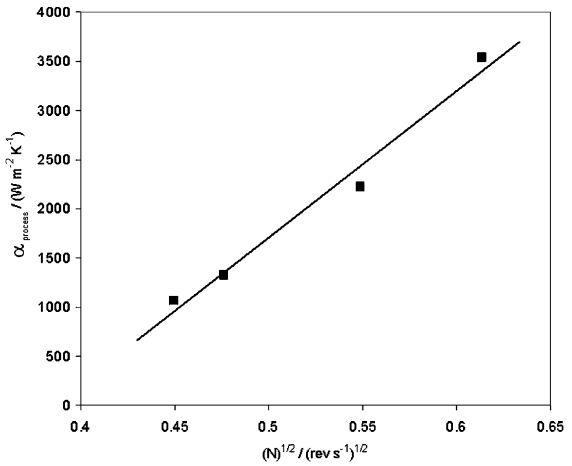

Fig. 12. Average process side heat transfer coefficient under crystallizing conditions as a function of the scraping rate.

lizer solid content. The fact that the intercept with the x-axis is located at 0.38 $(\text{rev s}^{-1})^{1/2}$ corresponding to a scraping rate of 0.14 rev s^{-1} implies that the mixing of the ice slurry at this stirrer speed is negligible.

The presence of a substantial amount of solids at eutectic conditions complicates the calculation of thermophysical properties of the crystallizer content. A heat transfer evaluation with dimensionless numbers like Reynolds and Prandtl has therefore not been performed.

6. Heat transfer in SCWC

6.1. SCWC coolant heat transfer characterization

Heat transfer characteristics of the coolant in the SCWC have been determined in experiments with constant process side conditions, i.e. constant scraping rate while coolant flow rates were varied in the range of 0.09–0.90 $\text{m}^3\,\text{h}^{-1}$ per cylinder. The constant factor in the Nu-relation for the coolant side was fitted using Eq. (24) and delivered the following results for inner and outer jacket respectively:

$$Nu_{\text{cool,inner}} = 0.024 \cdot Re^{0.8} \cdot Pr^{0.3} \tag{27}$$

$$Nu_{\text{cool,outer}} = 0.021 \cdot Re^{0.8} \cdot Pr^{0.3} \tag{28}$$

The cylinders each show slightly different behavior due to the geometrical differences. The fitted coefficients have a value which is close to the coefficient of 0.024 stated by Dittus and Boelter [9]. Therefore it is reasonable to assume the coolant flow within the cylinders to show turbulent behavior.

6.2. SCWC process heat transfer characterization

Knowing the resistances of the coolant and metal cylinder walls, the process side heat transfer characteristics have been determined at varying scraping rates for both the inner and the outer cooled cylinder wall. Experiments have been performed in which water and a HNO_3–KNO_3 solution was cooled from 17 to 8 °C at scraping rates ranging from 0.12 to 0.71 rev s^{-1}. Additionally the number of scrapers on the inner cylinder has been varied with two and four scraper blades. The validity of the penetration theory has been evaluated while an empirical Reynolds–Prandtl relation has also been derived.

6.3. SCWC heat transfer in non-crystallizing conditions

Penetration theory has been compared with experimental results in the same manner as described for the CDCC. The constant C_{pen} in Eq. (26) is calculated by regression for both inner and outer jacket. These are given in Table 4 including coefficients of determination.

Table 4
Fitted heat penetration constants for inner and out cooled wall in the SCWC

Parameter	Inner cylinder	Outer cylinder
C_{pen}	2.63	1.72
R^2	0.967	0.197

The time averaged crystallizer temperature in these experiments was 11 °C, therefore the physical properties required for calculation of the penetration model have been taken at this temperature. The penetration model predictions are represented by solid lines in Figs. 13 and 14, comparing them to experimental measurements. The

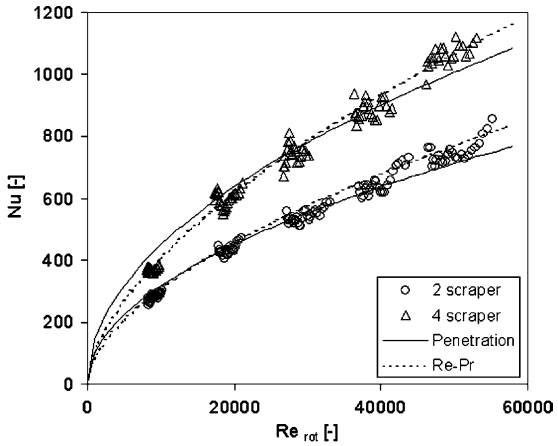

Fig. 13. Nu-numbers of the inner cylinder equipped with two or four blades as a function of rotational Re compared to penetration theory (solid lines) and Re–Pr-relations (dotted lines).

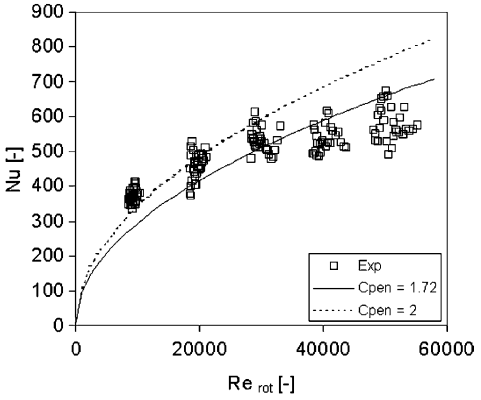

Fig. 14. Nu-numbers of the outer cylinder as a function of rotational Re compared to the fitted penetration theory $C_{\text{pen}} = 1.72$ (line) and the theoretical value $C_{\text{pen}} = 2$ (dotted line).

inner jacket heat transfer can be well described by penetration theory, although it is remarkable that the penetration constant is larger than the theoretical value of 2. From Fig. 14 it is clear that the measured data of the outer cooled wall show a trend which is not as steep as the penetration model predicts (line). At low scraper speed and thus low Reynolds numbers the data even seem to comply with the theoretical penetration theory ($C_{pen} = 2$), a trend which is broken at *Re*-numbers above 30 000. An explanation for this might be found in the geometry and construction of the scraper blades and the outer cylinder wall as depicted in Fig. 6.5. The eddies produced by the rotating scraper blades will flow towards the crystallizer wall instead of moving into the crystallizer to mix with the bulk. This effect might even be stronger at high rotational speeds due to the centrifugal forces exerted on the rotating liquid within the crystallizer. Thus heat transferred from the outer jacket will not be transported efficiently into the bulk. The mixing of the scraped stagnant layer and bulk is not optimal, which is assumed in penetration theory. Based on the heat transfer experiments a fit has been made for the constants in a Reynolds–Prandtl relation based on a linearized form of Eq. (23). Since especially the data of the outer wall heat transfer show a large bandwidth the degrees of freedom in the fit procedure have been narrowed down by setting the exponent of the Prandtl-term *b* to a value of 0.3. This value is commonly accepted in literature for expressing the dependence of heat transfer of thermophysical system properties [3–6]. The fit results for the inner and outer cylinder are shown in Table 5. The results for both inner jacket fits are presented in Fig. 13. The higher heat transfer coefficient as a result of a larger number of scraper blades on the inner jacket is expressed in the fit by a higher exponent of the Reynolds number. Although the fit for inner wall heat transfer is more accurate, penetration theory is preferred since this model automatically includes the effect of the number of scrapers. The outer wall is best approximated with the fitted *Re–Pr*-relation, although the R^2-value is still relatively low. The prediction of the *Re–Pr*-model for the outer wall is compared with the experimental data in Fig. 15. Model calculations are presented for each experimental data point, isothermal curves for the minimum and maximum temperatures of 10 and 17 °C are indicated by the lines.

Table 5
Fitted parameters in the Reynolds–Prandtl heat transfer relation for the SCWC

Parameter	Inner 2 scrapers	Inner 4 scrapers	Outer cylinder
a	0.57	0.60	0.26
b	0.30	0.30	0.30
C	0.829	0.830	18.38
R^2	0.990	0.990	0.837

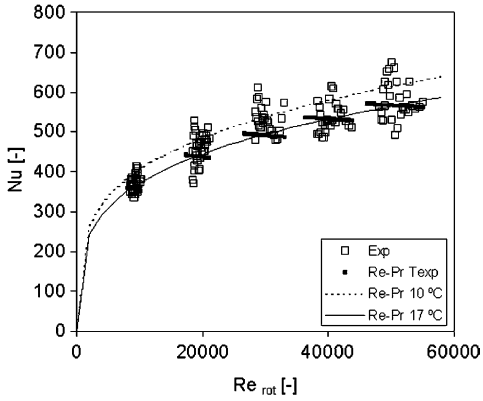

Fig. 15. Comparison of the fitted *Re–Pr*-model with experimental data of heat transfer water for the outer cylinder wall of the SCWC including isothermal *Re–Pr*-curves at 10 and 17 °C.

6.4. SCWC heat transfer in crystallizing conditions

Crystallizing experiments have been performed at logarithmic temperature differences varying from 2 to 7 K. Experiments at the largest temperature difference of 7 K were performed only using the outer wall as a cooled surface. Scraping rates were increased with increasing temperature differences from 0.56 to 1.07 rev s^{-1}. Measured heat fluxes through the inner and outer wall are presented in Fig. 16. The average overall heat transfer coefficient defined by the slope is 490 W m^{-2} K^{-1} for the outer wall and 585 W m^{-2} K^{-1} for the inner cylinder. It should however be noted that changes in heat flux are

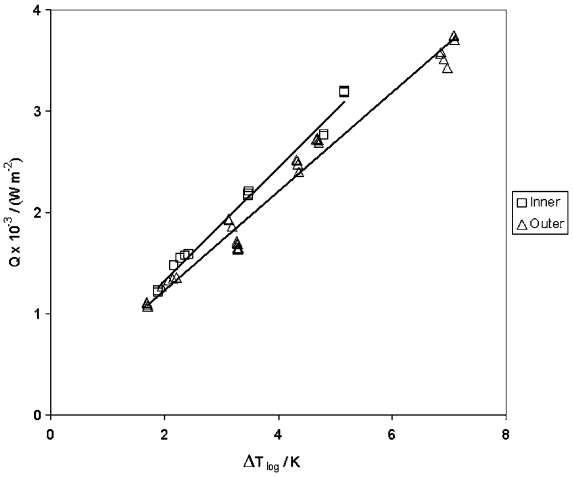

Fig. 16. Heat fluxes measured during crystallizing experiments in the SCWC.

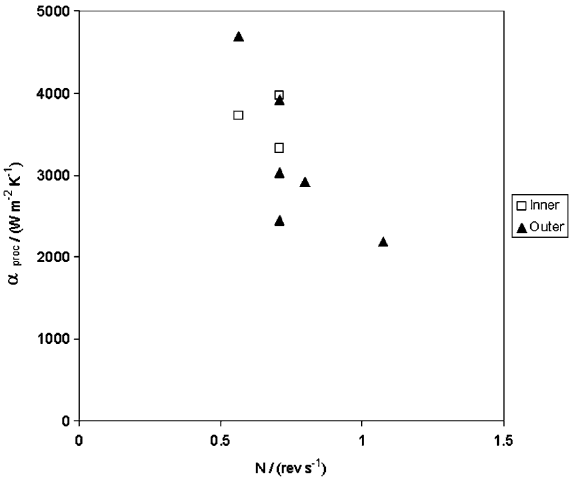

Fig. 17. Process side heat transfer coefficient of the SCWC in crystallizing conditions as a function of the scraping rate.

not only induced by the temperature difference in these data, since the scraping rate was varied simultaneously with the temperature difference. The effect of the scraping rate on the process side heat transfer coefficient is shown in Fig. 17. It is striking that the heat transfer coefficient decreases with increasing scraping rate and temperature difference. This is opposite to expectations, since generally a higher rotational speed leads to better mixing and therefore higher heat transfer rates. In this case however variations in the process bulk flow properties occur due changes in the solid content of ice within the crystallizer. At low logarithmic temperature differences the production rate of ice and salt are low producing an ice slurry containing approximately 6 vol.% solids. This amount increases to 10 vol.% at higher subcoolings. This change in solid content of the crystallizer affects heat transfer properties of the bulk substantially. Research into heat transfer rates of ice slurries in pipes and plate heat exchangers do not provide a consistent relation between heat flux and ice fraction [13–15]. It is therefore concluded that the influence of the ice fraction is dependent on crystal size, Reynolds number and the flow geometry. In this respect visual observations of the flow around the wing-like blade geometry of the scrapers shows that radial mixing within the crystallizer especially at higher solid contents is negligible. The increase of the amount of ice in the crystallizer at higher temperature differences usually leads to a more rapid consumption of supersaturation since there is more crystal surface available for growth. Opposite to this expectation the decrease of the heat transfer coefficient might indicate the presence of a thin insulating ice layer on the heat transfer surface due to inefficient ice removal by the scrapers. A combination of these phenomena might explain the lower observed heat transfer coefficients at higher scraping rates.

7. Conclusions

Heat transfer phenomena in two types of eutectic crystallizers have been analyzed. It was found that the coolant flow in the equipment can be described by fitted Dittus–Boelter relations, originally derived for turbulent flow within tubes. The Dittus–Boelter constant for the CDCC was best fitted at a value of 0.086. In the SCWC this constant was 0.024 and 0.021 for the inner and outer jacket respectively. For both crystallizers the transport of heat from process liquid to cooled wall surfaces at various rotational speeds of the scrapers can be accurately described with penetration theory. An exception should be made for the heat transfer of the outer jacket of the SCWC, which can be best approximated with a fitted *Re–Pr*-relation. In the CDCC heat transfer increases with increasing scraping rate in crystallizing conditions with a stable crystallizer solid content of approximately 8 wt.%. The height of the CDCC scraper blades provide a good ability to mix the produced ice slurry and thus promote heat transfer. This is not the case for the scrapers within the SCWC having a low wing-like geometry. As a result the increase of the ice content of the crystallizer probably dominates over the increase of scraper speed. The process side heat transfer therefore shows a decrease at higher temperature differences and scraping rates. The maximally measured process side heat transfer coefficient is slightly higher for the SCWC with a value of 4600 $W m^{-2} K^{-1}$ at a low temperature difference compared to 3600 $W m^{-2} K^{-1}$ for the CDCC. The total heat transfer rate is approximately equal for both crystallizers having values ranging from 500 to 700 $W m^{-2} K^{-1}$. Based on heat transfer rates there are no significant differences between the two types of tested crystallizers. Since the heat transfer resistance in the coolant has the same order of magnitude as the cooled metal plate and process fluid, the total heat transfer rate can be substantially increased when coolant flows are clearly situated in the turbulent flow regime instead of the transient regime.

References

[1] R. de Goede, E.J. de Jong, Heat transfer properties of a scraped-surface heat exchanger in the turbulent flow regime, Chem. Eng. Sci. 48 (1993) 1393–1404.
[2] A.M. Trommelen, W.J. Beek, H.C. van de Westelaken, Mechanism for heat transfer in a Votator-type scraped-surface heat exchanger, Chem. Eng. Sci. 26 (1971) 1987–2001.
[3] H. Abichandani, S.C. Sarma, Heat transfer and power requirements in horizontal thin film scraped surface heat exchangers, Chem. Eng. Sci. 43 (4) (1988) 871–881.
[4] H. Abichandani, S.C. Sarma, Heat transfer in horizontal mechanically formed thin-film heat exchangers—application

of penetration theory model, Int. J. Heat Mass Transfer 33 (1) (1990) 61–68.
[5] H. Miyashita, M. Yoshida, T. Yamane, Heat transfer correlation in high Prandtl (high Schmidt) number fluid in Votator type scraped surface heat exchanger, J. Chem. Eng. Jpn. 30 (3) (1997).
[6] M. Örvös, T. Balázs, K.F. Both, I. Csury, Investigation of heat transfer conditions in scraped surface heat exchanger, Period. Polytech. Ser. Mech. Eng. 38 (2–3) (1994) 123–138.
[7] D. Mann, LNG Materials and Fluids, National Bureau of Standards, Cryogenics Division, 1977.
[8] S. Kakaç, R.K. Shah, W. Aung, Handbook of Single-Phase Convective Heat Transfer, Wiley, New York, 1987.
[9] P.W. Dittus, L.M. Boelter, Heat transfer in automobile radiators of the tubular type, Int. Commun. Heat Mass Transfer 12 (1985) 3–22 (reprinted).
[10] W.J. Beek, K.M.K. Mutzall, Transport Phenomena, Wiley, New York, 1977.
[11] A.M. Trommelen, Physical aspects of scraped surface heat exchangers, Ph.D. thesis, Delft University of Technology, 1970.
[12] R. de Goede, Crystallization of paraxylene with scraped surface heat exchangers, Ph.D. thesis, Delft University of Technology, 1988.
[13] B.D. Knodel, D.M. France, U.S. Choi, M.W. Wambsganss, Heat transfer and pressure drop in ice-water slurries, Appl. Thermal Eng. 20 (2000) 671–685.
[14] J. Bellas, I. Chaer, S.A. Tassou, Heat transfer and pressure drop of ice slurries in plate heat exchangers, Appl. Thermal Eng. 22 (2002) 721–732.
[15] V. Ayel, O. Lottin, H. Peerhossaini, Rheology, flow behaviour and heat transfer of ice slurries. A review of the state of the art, Int. J. Refrig. 26 (2003) 95–107.